Local environment of Li intercalated in $Mo_6Se_zS_{8-z}$ as probed using electrochemical methods

L. S. Selwyn, W. R. McKinnon, J. R. Dahn,* and Y. Le Page
Solid State Chemistry Group, Division of Chemistry, National Research Council of Canada, Ottawa, Canada K1A 0R9
(Received 29 July 1985; revised manuscript received 9 December 1985)

Results are presented from electrochemical and *in situ* x-ray diffraction cells of the ternary molybdenum chalcogenides $Li_xMo_6Se_zS_{8-z}$ ($0 \le z \le 8$, $0 \le x \le 1$), where the $Mo_6Se_zS_{8-z}$ samples were obtained by chemical removal of Cu from $Cu_{2.5}Mo_6Se_zS_{8-z}$. The electrochemical results for the entire series can be accounted for with a lattice-gas model that assumes that the energy of a Li atom depends on the number of S and Se atoms nearby. This energy is dominated by the two nearest-neighbor chalcogens on the rhombohedral $\bar{3}$ axis. The analysis of the electrochemical results gives the fraction of the Se which resides in these sites. This fraction correlates well with the site occupancies refined from single-crystal x-ray diffraction. It is also accounted for by a model of crystal growth. Our models also account for the lattice expansions in some other Chevrel compounds $A_xMo_6Se_zS_{8-z}$ as a function of x and z.

I. INTRODUCTION

Lattice-gas models describe the thermodynamics of intercalation compounds, where the host is a framework containing interstitial sites into which atoms or molecules can be inserted reversibly. One of the parameters in these models is the "site energy," the energy of an isolated intercalant in the host relative to its energy outside. Although the site energy for binary hosts such as Mo_6Se_8 can be accurately measured,[1] it has never been calculated from first principles. It is not known, for example, whether only the host atoms adjacent to the intercalated atoms determine the site energy or whether more distant host atoms are also important.

In an attempt to answer this question, we studied the series of Chevrel phases $Li_xMo_6Se_zS_{8-z}$ with $0 \le x \le 1$ and $0 \le z \le 8$. We interpret the results with a lattice-gas model, similar to that used by McLennan[2] to discuss metal hydrides, which considers the change of energy of a Li atom when Se is substituted for S in the host. We find that the site energy is dominated by the two nearest chalcogen atoms, each of which is about ten times more important than any of the next-nearest chalcogens. Our results show that electrochemical methods can measure the distribution of host atoms which neighbor the intercalated lithium. In $Li_xMo_6Se_zS_{8-z}$, this distribution can be explained by a model that considers the energy of S and Se as the crystal grows.

II. STRUCTURE

The ternary molybdenum chalcogenides (Chevrel phases[3,4]) $A_xMo_6X_8$, where A is a metal atom and X is a chalcogen, are metallic and many are superconducting with high critical fields. Their room-temperature rhombohedral structure [space group $R\bar{3}$ (C_{3i}^2)] is made up of blocks of slightly distorted cubes or clusters of Mo_6X_8 units, with eight X atoms at the cube corners and six Mo atoms slightly outside the middle of the cube faces. These cubes are rotated by 25 to 27° about the $\bar{3}$ axis to optimize

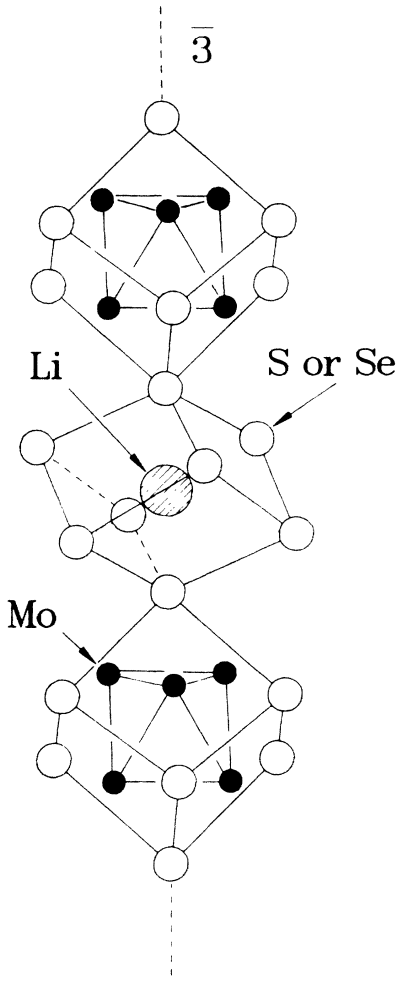

FIG. 1. Chevrel phase crystal structure ($\alpha_R < 93°$) stressing the local environment of eight chalcogens surrounding the lithium. In the text, the two chalcogens on the $\bar{3}$ axis surrounding the lithium are labeled X_a and the other six are labeled X_b.

the bonding distance between a chalcogen lying off the $\bar{3}$ axis and an Mo atom on an adjacent cube. A network of interconnecting channels parallel to the rhombohedral axes runs between the Mo_6X_8 clusters and contains the interstitial sites or cavities where the A atoms reside.

The sites used by the A atoms depend on the size of the rhombohedral angle α_R.[4] For large A atoms (i.e., Ag, La, Pb), α_R is small (89–93°) and each A is found at the symmetry center on the $\bar{3}$ axis in the middle of a cage formed by eight X atoms, each X from a different Mo_6X_8 unit, as shown in Fig. 1. There is one of these interstitial A atom sites per formula unit of Mo_6X_8. The cage of X atoms is a cube compressed along the $\bar{3}$ axis. Two of these chalcogens are on the $\bar{3}$ axis in the Wyckoff special positions $2c$, which we call X_a sites, and the remaining six chalcogens lie off the $\bar{3}$ axis in the general positions ($6f$) which we call the X_b sites. For smaller A atoms (i.e., Cu, Fe, Ni), α_R is larger (93–96°) and the A atoms are displaced from the $\bar{3}$ axis, and partially occupy one ring of six inner sites and one ring of six outer sites per formula unit of Mo_6X_8.

When α_R is small, the X_a site is significantly closer to the interstitial site than the X_b site is. As an example, in $Mo_6Se_4S_4$ where $\alpha_R \simeq 92°$, the X_a site is 2.3 Å away from the interstitial site, whereas the X_b site is 3.2 Å away. When α_R is larger, the difference in these distances is smaller. In $Cu_{2.5}Mo_6Se_2S_6$, where $\alpha_R \simeq 95°$, the X_a site is, respectively, 2.5 Å and 2.3–2.4 Å away from the inner and outer sites compared to 2.3 and 2.4 Å for X_b.

III. EXPERIMENTAL

The series of Chevrel compounds $Mo_6Se_zS_{8-z}$, $z=1$ to 7, were obtained by "indirect synthesis"[5] by preparing $Cu_{2.5}Mo_6Se_zS_{8-z}$ at 1250 °C and removing the Cu at room temperature. The starting materials were Mo wire (0.5 mm in diameter, Alfa Products, 99.9%), S lumps (Atomergic Chemetals, 99.9999%) or powder (Spex, 99.999%), Se pellets (Noranda, 99.999%), and Cu wire or sheets (ASARCO, 99.999%). The copper was first etched with a 50 vol%-50 vol% mixture of HNO_3 and H_2O. Stoichiometric quantities of the elements were placed in a quartz ampoule, filled with 30 kPa argon, heated from 200 °C to 1150 °C in 24 h, held at 1150 °C for 48 h, and cooled back to room temperature in 8 to 12 h. The samples were then shaken vigorously to expose unreacted Mo wire, and reheated twice to 1250 °C, each time heated to 1250 °C in 12 h, then held at 1250 °C for 30 h. The final product was single-phase as determined by x-ray powder diffraction. A Stoe Bragg-Brentano powder diffractometer and Ni-filtered Cu $K\alpha$ radiation[6] were used to obtain the powder diffraction data. Lattice parameters were determined by least squares refinement of the positions of 20 to 25 Bragg peaks.

To remove the copper, the Chevrel powders were reacted with an excess of 0.15M I_2 (0.30N) in acetonitrile[7,8] for about an hour at room temperature, filtered with excess CH_3CN and dried at 200 °C under flowing argon. Two samples, analyzed for Cu content using inductively coupled plasma atomic emission, had only residual amounts of copper: $Cu_{0.02}Mo_6Se_6S_2$ and $Cu_{0.006}Mo_6Se_2S_6$.

Electrochemical cells were constructed using these powders and Li metal foil.[9,10] The electrodes were separated by porous polypropylene film soaked in a solution of 1M $LiAsF_6$ (USS Agri-Chemicals) in distilled propylene carbonate. These cells were charged and discharged at constant current at 28.0±0.1 °C, and the voltage monitored as a function of time. These cells were first discharged to 1.6 V at a 5 or 10 h rate; that is, with a current such that either 5 or 10 h were needed for $\Delta x = 1$. Copper is forced out of the host by Li near 1.85 V,[11] and $-(\partial x/\partial V)_T$ has a peak at that voltage when the host still contains Cu. Copper removal using the iodine solution was repeated a second time if residual copper was observed in $-(\partial x/\partial V)_T$. A typical discharge and charge cycle is shown in Fig. 2 as a plot of $-(\partial x/\partial V)_T$ versus voltage (V). After this initial cycle, the cells were cycled over the upper voltage range (the smaller peak in Fig. 2), at a 40-h rate.

In the compounds with $z=2$ and $z=6$, *in situ* x-ray diffraction cells with Be x-ray windows were prepared as in Ref. 12. The cells were held at some voltage until the current had dropped below a 250-h rate, then the x-ray diffraction profiles were recorded at 23±1 °C.

Figure 3 shows the rhombohedral lattice parameters α_R and a_R for the host materials $Mo_6Se_zS_{8-z}$ ($z=0$ to 8) prepared by indirect synthesis. These parameters and the cell volume are listed in Table I. Results obtained previously by Chevrel and Sergent[5] and by Tarascon *et al.*[13] have been included in Fig. 3. Our results are in good agreement with those of Tarascon *et al.*,[13] whose samples were prepared by chemical removal of the Cu from $Cu_2Mo_6Se_zS_{8-z}$ made at 1200 °C. The results from Chevrel and Sergent[5] agree with our results except for the cell edge between $z=4$ and 7. Their samples were prepared by indirect synthesis but no further experimental details were provided.

The rhombohedral lattice parameters α_R and a_R, obtained as a function of x from *in situ* x-ray cells $Li/Li_xMo_6Se_6S_2$ and $Li/Li_xMo_6Se_2S_6$ at 23 °C, are shown in Fig. 4 and in Table II. Similar to $Li_xMo_6Se_8$ (Refs. 1 and 14) and $Li_xMo_6S_8$ (Ref. 15) at room temperature, these compounds expand and remain a single phase as

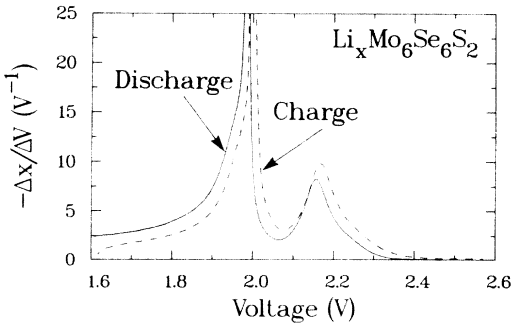

FIG. 2. Plot of $-(\partial x/\partial V)_T$ versus voltage for a $Li/Li_xMo_6Se_6S_2$ electrochemical cell at 28 °C. The current used to discharge and charge this cell corresponded to a 10-h rate. These curves are typical of those recorded for electrochemical cells in the series $Li/Li_xMo_6Se_zS_{8-z}$ for $0 \le x \le 4$ and $1 \le z \le 7$.

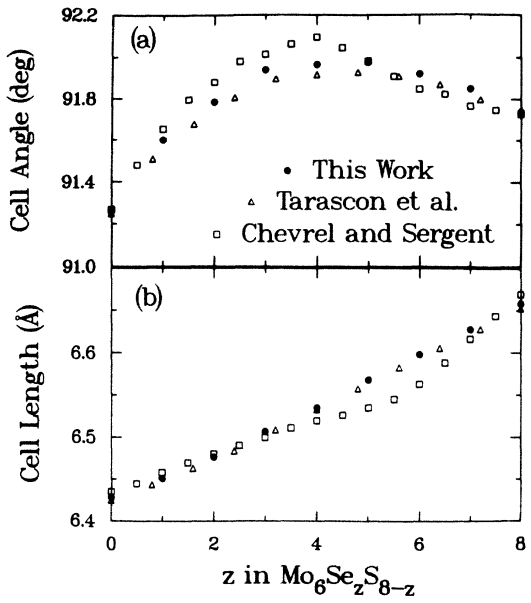

FIG. 3. Rhombohedral unit-cell lattice parameters as a function of selenium content in $Mo_6Se_zS_{8-z}$. (a) Rhombohedral unit-cell angle; (b) length of rhombohedral cell edge. Solid circles for this work (see Table I), obtained using powder x-ray diffraction at 23 °C, have error limits within the size of the symbols. Open triangles from Tarascon *et al.*[13] and open squares from Chevrel and Sergent.[5]

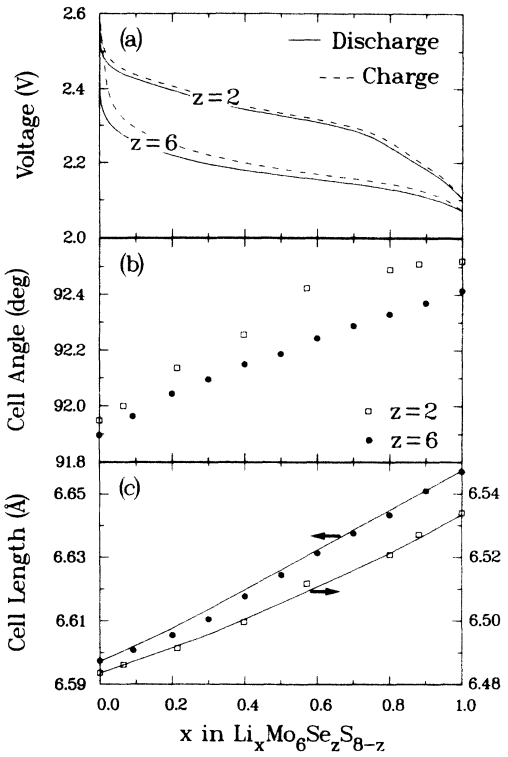

FIG. 4. Voltage curves and variation of rhombohedral lattice parameters as a function of x, the lithium content, from electrochemical cells of $Li/Li_xMo_6Se_6S_2$ and $Li/Li_xMo_6Se_2S_6$. (a) Voltage versus x at 28 °C obtained at a 40-h rate. Rhombohedral unit-cell angle (b) and length of cell edge (c), at 23 °C from *in situ* x-ray diffraction, are tabulated in Table II. The solid curves in (c) are calculated theoretically, as discussed in the text.

they are intercalated with lithium to $x = 1$. Moreover, the Bragg peaks remain resolution-limited for all $x \leq 1$, showing that Li is homogeneously distributed through the host. (The experimental sensitivity to deviations in x is about 0.02.) The small difference in lattice parameters for $Mo_6Se_2S_6$ listed in Tables I and II reflects different amounts of residual copper in the samples. Since $\alpha_R < 93°$, we expect that the Li atoms occupy the interstitial sites on the $\bar{3}$ axis as shown in Fig. 1.

The results from single-crystal x-ray studies on $Cu_{2.5}Mo_6Se_4S_4$, $Mo_6Se_4S_4$, and $Cu_{2.5}Mo_6Se_6S_2$ are summarized in Tables III and IV. The three crystals belonged to the rhombohedral space group $R\bar{3}$ (C_{3i}^2), as determined from the refinement of about 560 measured reflections

TABLE I. Rhombohedral lattice parameters for $Mo_6Se_zS_{8-z}$.

z	Cell edge (Å) (±0.001)	Cell angle (deg) (±0.01)	Cell volume (Å^3) (±0.1)
0	6.428	91.26	265.4
1	6.452	91.60	268.2
2	6.477	91.79	271.4
3	6.508	91.94	275.1
4	6.536	91.97	278.7
5	6.568	91.98	282.9
6	6.599	91.92	286.8
7	6.628	91.85	290.7
8	6.659	91.74	294.8

TABLE II. Rhombohedral lattice parameters for $Li_xMo_6Se_6S_2$ and $Li_xMo_6Se_2S_6$.

x	Cell edge (Å) (±0.001)	Cell angle (deg) (±0.01)	Cell volume (Å^3) (±0.1)
		$Li_xMo_6Se_6S_2$	
0.00	6.597	91.90	286.6
0.09	6.601	91.96	287.1
0.20	6.606	92.04	287.6
0.30	6.611	92.10	288.3
0.40	6.618	92.15	289.2
0.50	6.624	92.19	290.0
0.60	6.631	92.24	290.1
0.70	6.638	92.29	291.7
0.80	6.643	92.33	292.4
0.90	6.651	92.37	293.4
1.00	6.657	92.94	294.2
		$Li_xMo_6Se_2S_6$	
0.00	6.484	91.95	272.1
0.07	6.486	92.00	272.3
0.21	6.491	92.14	272.9
0.40	6.500	92.26	273.9
0.57	6.512	92.42	275.3
0.80	6.521	92.49	276.4
0.88	6.527	92.51	277.2
1.00	6.534	92.52	278.1

TABLE III. Structural parameters obtained from single-crystal x-ray diffraction for $Cu_{2.5}Mo_6Se_4S_4$, $Cu_{2.5}Mo_6Se_6S_2$, and $Mo_6Se_4S_4$. The interatomic distances are accurate to the last digit quoted. Se indicates sites containing Se or S with Se(1) corresponding to an X_b site and Se(2) to an X_a site. The copper sites, labeled Cu(1) and Cu(2), are respectively, one of six outer or six inner interstitial sites. The densities (ρ) are calculated using the chemical formulas shown.

	$Cu_{2.5}Mo_6Se_4S_4$	$Mo_6Se_4S_4$	$Cu_{2.5}Mo_6Se_6S_2$
Mo-Mo (Å)	2.68/2.72/3.39	2.71/2.85/3.15	2.68/2.72/3.45
Mo-Se (Å)	2.48-2.57	2.48-2.55	2.53-2.63
Shortest Se-Se (Å)	3.47	3.30	3.51
Cu(1)-Se(1) (Å)	2.51/2.34/2.29		2.45/2.42/2.34
Cu(1)-Se(2) (Å)	2.34		2.39
Cu(2)-Se(1) (Å)	2.24/2.33		2.33/2.43
Cu(2)-Se(2) (Å)	2.52/2.43		2.50/2.45
Se(1)-Li site (Å)	3.32	3.15	3.34
Se(2)-Li site (Å)	2.05	2.27	2.12
Crystal size (mm)	$0.1\times0.1\times0.1$	$0.07\times0.07\times0.07$	$0.7\times0.10\times0.15$
a_R (Å)	6.645(2)	6.521(2)	6.730(1)
α_R (deg)	95.16(2)	91.92(2)	94.98(1)
ρ ($g\,cm^{-3}$)	6.758	6.117	7.022
Residual R (%)	3.0	5.86	4.5
Residual Rw (%)	2.4	5.23	4.7
Observed reflections for Rw ($>2\sigma$)	465	452	535

from graphite-monochromatized Mo $K\alpha$ x-rays up to $2\theta=60°$. An absorption correction made by Gaussian integration was applied to the refinement of $Cu_{2.5}Mo_6Se_4S_4$ but not of $Cu_{2.5}Mo_6Se_6S_2$, because the latter crystal was imbedded in glue and not limited by faces. The $Mo_6Se_4S_4$ crystal was small and had a random shape so no absorption correction was made. The mosaic spread of $Mo_6Se_4S_4$ was about 0.5°, presumably the result of damage when the copper was removed chemically, and difference-Fourier maps showed no residual electron density at the copper sites.

The atomic positions listed in Table IV were refined assuming that the chalcogen sites were occupied by Se only, but with fractional occupancy. The positional and thermal parameters were then fixed and the occupancies of chalcogen sites by S or Se were refined, constrained to full occupancy of the eight available sites. The mean of the principal axes of the thermal ellipsoid, B_{iso}, was calcu-

TABLE IV. Site occupancy, atom positions, and thermal parameters obtained from single-crystal x-ray diffraction. The chemical formulas in brackets are calculated from the refinement. The chalcogen and copper sites are labeled as in Table III. The standard deviation for the last printed digit is shown in brackets.

	Site	Occupancy	x	y	z	B_{iso} (Å^2)
		(a) $Cu_{2.5}Mo_6Se_4S_4$ ($Cu_{2.6}Mo_6Se_{3.4}S_{4.6}$)				
Mo	6*f*	1	0.2282(1)	0.4080(1)	0.5424(1)	0.62(5)
Se(1)/S(1)	6*f*	0.35(2)/0.65	0.3755(3)	0.1288(3)	0.7239(4)	1.0(1)
Se(2)/S(2)	2*c*	0.63(2)/0.37	0.1970(2)	0.1970	0.1970	0.9(1)
Cu(1)	6*f*	0.20(2)	0.6421(1)	0.0479(1)	−0.0126(1)	3.5(3)
Cu(2)	6*f*	0.23(2)	0.0986(1)	0.8338(1)	0.0521(1)	4.6(4)
		(b) $Mo_6Se_4S_4$ ($Mo_6Se_{3.6}S_{4.4}$)				
Mo	6*f*	1	0.2162(3)	0.4073(3)	0.5485(3)	0.52(6)
Se(1)/S(1)	6*f*	0.37(4)/0.63	0.3806(5)	0.1284(5)	0.7430(5)	0.9(1)
Se(2)/S(2)	2*c*	0.70(4)/0.30	0.2084(4)	0.2084	0.2084	1.0(1)
		(c) $Cu_{2.5}Mo_6Se_6S_2$ ($Cu_{2.6}Mo_6Se_{6.5}S_{1.5}$)				
Mo	6*f*	1	0.2314(1)	0.4101(1)	0.5422(1)	0.55(4)
Se(1)/S(1)	6*f*	0.77(2)/0.23	0.3743(3)	0.1272(3)	0.7253(4)	1.1(1)
Se(2)/S(2)	2*c*	0.91(2)/0.09	0.2004(3)	0.2004	0.2004	1.2(1)
Cu(1)	6*f*	0.23(2)	0.6332(1)	0.0486(1)	−0.0233(1)	4.8(4)
Cu(2)	6*f*	0.21(2)	0.0929(1)	0.8525(1)	0.0464(1)	5.5(5)

lated from the anisotropic thermal motion refined for all atoms and is listed in Table IV.

The features for the electrochemical cell $Li/Li_xMo_6Se_6S_2$ shown in Fig. 2 are typical for the intermediate members in the series $Li_xMo_6Se_zS_{8-z}$. The smaller peak at higher voltage arises from the filling of the sites on the $\bar{3}$ axis ($0 \le x \le 1$) in the rhombohedral phase with α_R about 92°, where there is one interstitial site per formula unit of host. The larger peak at lower voltage corresponds to a structural phase transition to another rhombohedral phase where α_R opens to about 94° to accommodate lithium atoms into one of twelve interstitial sites per formula unit of host. Additional peaks, associated with triclinic and incommensurate lattice distortions,[14,15] have been observed near 1.81 and 1.83 V in $Li/Li_xMo_6S_8$ and near 1.90 and 1.69 V in $Li/Li_xMo_6Se_8$. These peaks are not observed in any of the intermediate members in the series.

To correct for material that was not electrically connected to the cathode, the x values used in Fig. 4 were obtained by normalizing the electrochemical cell data to $x=0$ at 2.6 V and to $x=1$ at a voltage between 2.0 and 2.1 V. The voltage limit for $x=1$ was chosen to correspond to the minimum in $-(\partial x/\partial V)_T$ just above the peak at 2 V (see Fig. 2). The solid lines in Fig. 4(c) were calculated as discussed later.

The voltage as a function of x for the series $Li_xMo_6Se_zS_{8-z}$, with $x=0$ to 1 and $x=0$ to 8, is shown in Fig. 5. These voltage curves have been normalized to $x=0$ at 2.6 V and $x=1$ as described above. The curves for $z=0$ and $z=8$ were taken from previous studies on $Li_xMo_6Se_8$ (Refs. 1 and 14) and $Li_xMo_6S_8$.[15] The average voltage decreases as z increases and the voltage varies more rapidly with x for $1 \le z \le 7$ than for $z=0$ or $z=8$.

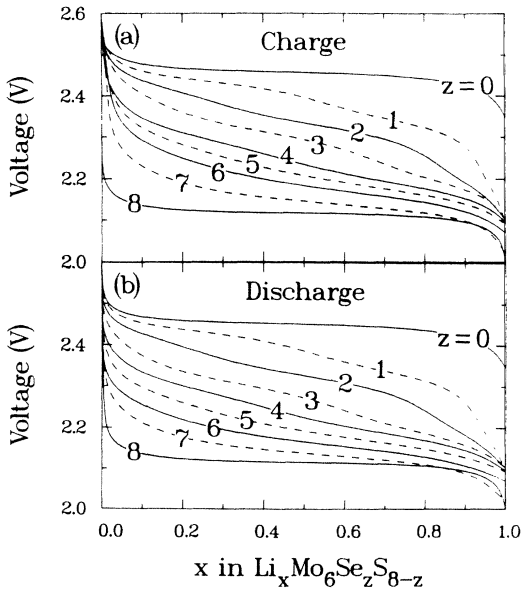

FIG. 5. Voltage versus lithium concentration from electrochemical cells of $Li/Li_xMo_6Se_zS_{8-z}$ for $0 \le x \le 1$ and $0 \le z \le 8$ at 28 °C. The current for $z=1, \ldots, 7$ corresponded to a 40-h rate. Curves for $z=0$ and $z=8$ were taken from Ref. 15 and Ref. 14, respectively.

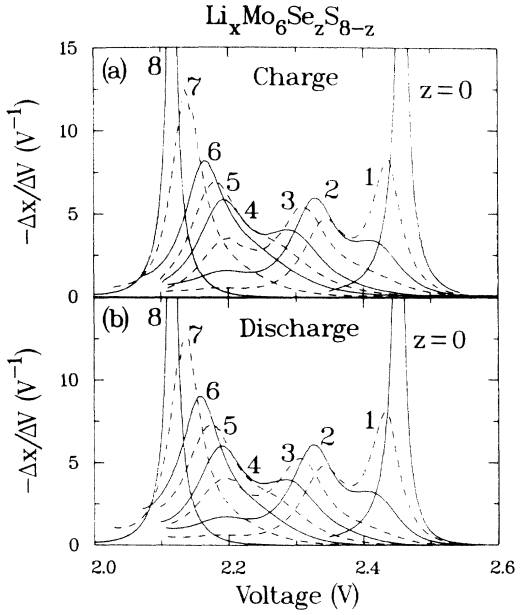

FIG. 6. Curves of $-(\partial x/\partial V)_T$ versus voltage at 28 °C for electrochemical cells $Li/Li_xMo_6Se_zS_{8-z}$ using results from Fig. 5.

The curves in Fig. 5 for $1 \le z \le 7$ are not smooth but have steps. These steps appear as peaks in the derivative $-(\partial x/\partial V)_T$, as is shown versus V in Fig. 6. When $z=0$, $-(\partial x/\partial V)_T$ shows a single peak near 2.45 V. As z increases, this peak shrinks, a second peak appears near 2.3 V and a third one near 2.2 V. Eventually, the third peak moves to 2.1 V where, for $z=8$, it is the only peak.

The symbols in Fig. 7 show the areas under each of the peaks in Fig. 6 as a function of z. (The solid curves were calculated, as described later.) We estimated these areas by assuming that each peak extends between the minima

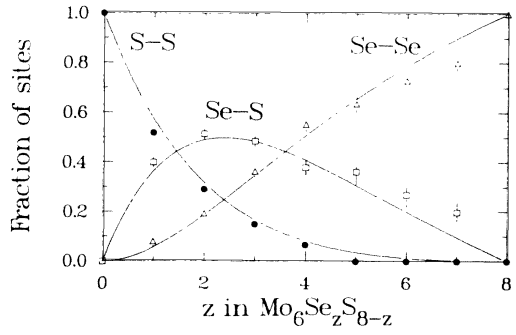

FIG. 7. Fraction of sites, containing either 0, 1, or 2 selenium atoms in the two chalcogen sites on the rhombohedral $\bar{3}$ axis, plotted versus z, the total selenium concentration in $Mo_6Se_zS_{8-z}$. Solid circles (S:S), open squares (Se:S), and open triangles (Se:Se) obtained from the area under the peaks shown in Fig. 6 as described in the text. Solid lines are predicted using a crystal growing energy $\varepsilon = 1.2kT_g$, in the crystal growing model described in the text.

in its second derivative. For the theoretical calculations discussed below, this procedure gives the areas to ±2%.

IV. LATTICE-GAS MODELS

A. Multiple lithium sites

The voltage V in an electrochemical cell is related to the chemical potential μ of an intercalated Li atom in a host material (cathode) by $V=-(\mu-\mu_0)/e$, where $-e$ is the charge on an electron and μ_0 is the chemical potential of Li in Li metal (anode). For many intercalation compounds, μ can be calculated using lattice-gas models.[16] We extend the lattice-gas model used to describe the behavior of mobile lithium atoms in $Li_xMo_6Se_8$,[1] where the host has one kind of interstitial site, to a system where the host contains several kinds of interstitial sites.

Let each kind of site be labeled by α and let p_α be the fraction of sites of kind α, and x_α the fraction of α sites occupied by Li. Then the overall fraction of sites occupied by Li is

$$x=\sum_\alpha p_\alpha x_\alpha \ . \tag{1}$$

We take the site energy for an α site to be ε_α, and we assume the interaction between intercalated atoms can be described by mean-field theory with a single interaction U, so the interaction energy per site is $Ux^2/2$. Thus the total energy E for a lattice of N sites is given by

$$\frac{E}{N}=\sum_\alpha p_\alpha \varepsilon_\alpha x_\alpha+\tfrac{1}{2}Ux^2 \ . \tag{2}$$

The entropy S is given by

$$-\frac{S}{Nk}=\sum_\alpha p_\alpha[x_\alpha \ln x_\alpha+(1-x_\alpha)\ln(1-x_\alpha)] \ . \tag{3}$$

The chemical potential μ_α of a particle on an α site is the derivative of $E-TS$ with respect to $n_\alpha=Nx_\alpha p_\alpha$, the number of atoms on α sites:

$$\mu_\alpha=\varepsilon_\alpha+Ux+kT\ln\left[\frac{x_\alpha}{1-x_\alpha}\right] \ . \tag{4}$$

Note that the interaction term in this equation involves x. At equilibrium, all chemical potentials μ_α are equal to the same value, μ.

These equations can be solved numerically for x_α. The inverse derivative $(\partial x/\partial\mu)_T$ can be written as

$$\left[\frac{\partial x}{\partial\mu}\right]_T=-\frac{1}{e}\left[\frac{\partial x}{\partial V}\right]_T=\left[U+\frac{kT}{\sum_\alpha p_\alpha[x_\alpha(1-x_\alpha)]}\right]^{-1} \ . \tag{5}$$

The results reduce to those in Ref. 1 for a single type of site.

When the difference in site energies ε_α are large compared to kT, Eq. (5) gives a series of peaks. The width of these peaks in $(\partial x/\partial\mu)_T$ is set by $p_\alpha U/kT$ rather than only U/kT. Suppose a particular site α' is filling and the others $\alpha'\neq\alpha$ are either all full or all empty. Then

$$\left[\frac{\partial x}{\partial\mu}\right]_T\simeq\left[U+\frac{kT}{p_\alpha[x_\alpha(1-x_\alpha)]}\right]^{-1}$$
$$=p_\alpha\left[p_\alpha U+\frac{kT}{[x_\alpha(1-x_\alpha)]}\right]^{-1} \ . \tag{6}$$

For $U=0$, the height of the peak is reduced by a factor p_α over the case of a single site. When U is nonzero, the width of the peak is set by the parameter $p_\alpha U/kT$. When U/kT is near -4, the change in peak width on going from a single site to many sites can be large. Figure 8 shows a system with two kinds of sites $\alpha=1$ and 2 for the three cases $p_1=0$, $p_1=\frac{1}{2}$, and $p_1=1$. The two peaks present for $p_1=\frac{1}{2}$ are about 7 times broader than the single peaks in the other two cases even though U is the same in all three cases.

We now apply these results to the Chevrel compounds when the rhombohedral angle α_R is small (Fig. 1). We assume that the site energy is linearly related to the number n_a and n_b of Se atoms in X_a sites (on the $\bar{3}$ axis) and in X_b sites (off the $\bar{3}$ axis):

$$\varepsilon_\alpha=\varepsilon(n_a,n_b)=\varepsilon_0+n_a\varepsilon_a+n_b\varepsilon_b \ . \tag{7}$$

Here ε_0 is the Li site energy when all eight chalcogens are sulfur, ε_a is the contribution to the Li site energy when one S in site X_a is replaced by one Se, and ε_b is the contribution to the Li site energy when one S in site X_b is replaced by one Se. The total number of Se in sites X_a and X_b is given by n_a and n_b, respectively.

The probability p_α of the Li site $\alpha=(n_a,n_b)$ is given by

$$p_\alpha=p_a(n_a)p_b(n_b) \ , \tag{8}$$

where $p_a(n_a)$ and $p_b(n_b)$ are the probabilities that a given interstitial site has n_a Se atoms on the $\bar{3}$ axis or n_b Se atoms off the $\bar{3}$ axis, respectively. For given values of the average number of Se on and off the $\bar{3}$ axis, z_a and z_b, respectively, these probabilities are:

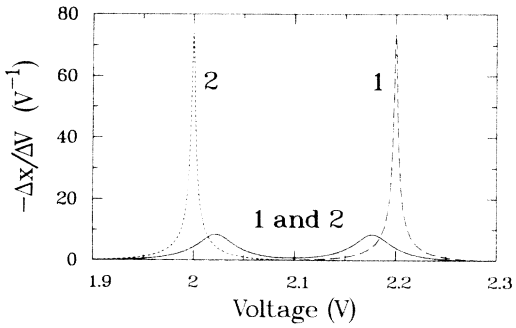

FIG. 8. Predicted curves for $-(\partial x/\partial V)_T$ versus voltage using a lattice-gas model. The solid curve is predicted using a hypothetical host lattice containing equal numbers of two types of sites, 1 and 2, with site energies $\varepsilon_1=-2.2$ eV and $\varepsilon_2=-2.0$ eV, and $U=-0.0904$ eV. The broken curves show the corresponding predicted curves using the host lattice with only one site energy (either 1 or 2).

$$p_a(n_a)=\frac{2!}{n_a!(2-n_a)!}z_a^{n_a}(1-z_a)^{2-n_a}\ , \tag{9}$$

$$p_b(n_b)=\frac{6!}{n_b!(6-n_b)!}z_b^{n_b}(1-z_b)^{6-n_b}\ . \tag{10}$$

B. Chalcogen sites

At room temperature, the Se and S atoms are frozen into sites in the crystal, so they entered the lattice-gas model above only through the model parameters. At the temperature T_g at which the crystal grows (where no Li is present), the S and Se are presumably mobile, so we can consider a second lattice-gas model to describe how S and Se are incorporated in X_a and X_b sites. (Note that we cannot consider a lattice-gas model that treats S, Se, and Li on an equal footing, because all three types of atoms are never simultaneously present and mobile.)

We assume each site on the chalcogen lattice can be occupied only by S or Se; vacancies are neglected. Then we have a lattice gas with two kinds of sites, so we can use Eqs. (1) to (4). The chemical potential ν (the change in free energy when S is replaced by Se) is given by

$$\nu=kT_g\ln\left[\frac{z_a}{1-z_a}\right] \tag{11}$$

and

$$\nu-\varepsilon=kT_g\ln\left[\frac{z_b}{1-z_b}\right]\ , \tag{12}$$

where z_a and z_b are the fractions of selenium in the X_a and X_b sites. The energy ε is that required to interchange a Se in site X_a and a S in site X_b. Equations (11) and (12) can be solved for z_a and z_b in terms of ε and $z=2z_a+6z_b$, although in practice it is simpler to calculate z_a and z_b for a series of values of ν. When $\varepsilon>0$, then Se sits preferentially in the X_a sites on the $\bar{3}$ axis.

V. RESULTS AND DISCUSSION

A. Chalcogen ordering

The presents of three peaks in $-(\partial x/\partial V)_T$ in Fig. 6 suggests there are three different types of sites for Li in $Li_xMo_6Se_zS_{8-z}$. The closest chalcogens to the lithium site are the two chalcogens on the $\bar{3}$ axis and there are only three possible combinations of chalcogens (Se:Se, Se:S, and S:S) on pairs of these sites. Therefore, our results imply that the dominant term in the lithium site energy is $n_a\varepsilon_a$ [Eq. (7)] from the chalcogens in sites X_a.

The total area under each peak in Fig. 6, plotted in Fig. 7, gives the fraction of Li sites surrounded by 0, 1, or 2 Se atoms on the $\bar{3}$ axis [$p_a(n_a)$ in Eq. (9)]. For a given z, the peaks at low voltages, due to two Se atoms at X_a, are stronger than expected if Se showed no preference for X_a sites over X_b sites. For example, when $z=4$, about 50% of the Li sites are surrounded by Se:Se in the two X_a sites, 40% with with Se:S, and the remaining 10% with S:S. If the Se did not prefer X_a sites over X_b sites, then the distribution would have been 25% Se:Se, 50% Se:S, and 25% S:S. This preference of Se over S for sites on the $\bar{3}$ axis implies $\varepsilon>0$ in the crystal growing model described in the previous section. The solid curves in Fig. 7 were determined from $p_a(n_a)$ calculated from Eq. (9), with z_a calculated from Eqs. (11) and (12) for $\varepsilon=1.2kT_g$.

Nonrandom chalcogen arrangements have been observed in other Chevrel compounds. Perrin *et al.*,[17] using single-crystal x-ray diffraction, found all the bromine atoms in $Mo_6S_6Br_2$ to be ordered at the X_a sites. Neutron powder-diffraction data[18] on $AMo_{6.05+z}S_8O_z$ ($0\le z\le 0.2$, A=Sn, Pb) showed that all the oxygen atoms were on the $\bar{3}$ axis in the X_a sites. Delk and Sienko,[19] suggesting that the chalcogen sites on or off the $\bar{3}$ axis were chemically different, explained their x-ray diffraction data on $SnMo_6S_{8-z}$ ($0\le z\le 2$) (Ref. 19) by placing the sulfur vacancies on the $\bar{3}$ axis. They explained the x-ray diffraction results on $PbMo_6Se_zS_{8-z}$ (Ref. 20) as an excess of S, not Se, on the $\bar{3}$ axis. Recent work by Tarascon *et al.*[21] on $YbMo_6Se_zS_{8-z}$ and by Johnson *et al.*[22] on $AMo_6Se_zS_{8-z}$ where A=La, Sm, Eu, Yb, Pb, and Ag, provided further x-ray evidence to support the ordering of S, not Se, on the $\bar{3}$ axis. This ordering was found to be strongest in La and weakest in Ag, where the distribution appeared to be almost random.

The apparent discrepancy between our work, where Se prefers sites on the $\bar{3}$ axis, and other work where S prefers those sites, is related to the preparation of the Chevrel phases. In the samples where sulfur prefers the X_a sites, the metal atom content A was one (i.e., $A_1Mo_6Se_zS_{8-z}$), α_R was small (89° to 93°), there was only one interstitial site on the $\bar{3}$ axis per formula unit of host, and the interstitial A atom was closer to the chalcogens in the X_a sites than in the X_b sites.[5] In these compounds, S prefers to occupy the chalcogen site on the $\bar{3}$ axis where it can be closer to the interstitial A atom.

In this work, the $Cu_{2.5}Mo_6Se_zS_{8-z}$ compounds have a larger rhombohedral angle, ~95°, and the copper atoms are distributed in the rings of six inner and six outer interstitial sites. The copper atoms on the inner sites [Cu(2) in Table IV] are, on the average, about 0.1 to 0.2 Å closer to the chalcogen in the X_b sites [Se(1) in Table IV] than to the chalcogens in the X_a sites [Se(2) in Table IV]. The copper atoms on the outer sites [Cu(1) in Table IV] are about equally distant from the X_a and X_b sites. Thus the sulfur atoms still prefer to occupy chalcogen sites closer to the A atoms; but now these sites are X_b instead of X_a. Since sulfur prefers the X_b sites, Se is forced into X_a. The distribution of S and Se is frozen into the crystal at room temperature so Se remains preferentially on the $\bar{3}$ axis when Cu is removed.

Single-crystal x-ray diffraction studies confirmed the preference of Se for the X_a sites (Table IV). In $Cu_{2.5}Mo_6Se_4S_4$, the refined value $z_a=0.63(2)$ is comparable to the predicted value of $z_a=0.71$ (from Fig. 7) for this formula and agrees better with the predicted value of 0.63 corresponding to the refined stoichiometry $Cu_{2.6}Mo_6Se_{3.4}S_{4.6}$. Similarly, for the single crystal of $Cu_{2.5}Mo_6Se_6S_2$, $z_a=0.91$ is comparable to the predicted value $z_a=0.88$ (from Fig. 7) for this formula and also agrees better with the value $z_a=0.92$ obtained for the refined crystal stoichiometry $Cu_{2.6}Mo_6Se_{6.5}S_{1.5}$.

A single-crystal x-ray refinement on $Mo_6Se_4S_4$ showed that the atom positions and the occupancies of Se and S had not changed much when the Cu was removed (Table IV). Although these results on $Mo_6Se_4S_4$ are not as reliable as those for $Cu_{2.5}Mo_6Se_4S_4$ and $Cu_{2.5}Mo_6Se_6S_2$ because of the poor crystal quality found after chemical removal of the copper, the refined occupancy agrees with the predicted occupancy 0.68 from the refined formula $Mo_6Se_{3.6}S_{4.4}$. The observed cell parameters also agree with the values $a_R = 6.525$ Å and $\alpha_R = 91.96°$ interpolated from Table I for the refined formula.

B. Predicted curves for $-(\partial x/\partial V)_T$ versus V

To calculate $-(\partial x/\partial V)_T$ from Eq. (5), we assume that the values of z_a and z_b for a given z are given by Eqs. (11) and (12), with $\varepsilon = 1.2kT_g$. Most other constants we need come from results for $z=0$ and $z=8$. Previous electrochemical results on $Li_xMo_6Se_8$ (Ref. 1) have been described accurately using Eqs. (4) and (5) with one site energy and with an interaction $U=-0.0904$ eV. In $Li_xMo_6S_8$,[23] U is within 10% of this value. Because of this similarity, we set $U=-0.0904$ eV for the whole series $Li_xMo_6Se_zS_{8-z}$. The peaks in $-(\partial x/\partial V)_T$ (Fig. 6) occur at 2.455 V in $Li_xMo_6S_8$ and at 2.117 V in $Li_xMo_6Se_8$. For $Li_xMo_6S_8$, the peak should be at $\mu = -eV = \varepsilon_0 + U/2$, which implies $\varepsilon_0 = 2.410$ eV and for $Li_xMo_6Se_8$, the peak occurs at $\mu = \varepsilon_0 + 2\varepsilon_a + 6\varepsilon_b + U/2$ so ε_a and ε_b must satisfy $2\varepsilon_a + 6\varepsilon_b = 0.338$ eV $= 13.025kT$. The only remaining parameter in the lattice-gas model is the ratio $\varepsilon_a/\varepsilon_b$. Choosing this ratio to be equal to 10 (i.e., $\varepsilon_a = 5.01kT$ and $\varepsilon_b = 0.501kT$) best fits the data.

Figure 9(a) shows the curves calculated using Eqs. (4) and (5). The calculation describes the relative heights and positions of the peaks in $-(\partial x/\partial V)_T$ but for $z=1$, 2, and 3, predicts peaks that are overly sharp. A less negative value of U describes the peaks for $z=1$, 2, and 3 better, but the other peaks less well. Figure 9(b) shows the calculations for $U=-0.030$ eV using $\varepsilon_0 = -2.440$ eV to match the peak position for $z=0$. The values of ε_a and ε_b were kept the same as in Fig. 9(a).

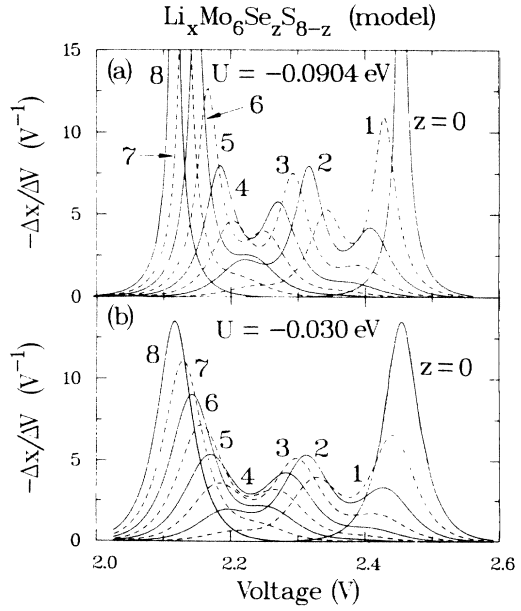

FIG. 9. $-(\partial x/\partial V)_T$ versus voltage for the series $Li_xMo_6Se_zS_{8-z}$ predicted with the lattice-gas model described in the text with (a) $U=-0.0904$ eV and (b) $U=-0.030$ eV.

Both values of U show the same features that reproduce the experimental curves: three peaks corresponding to the three possible arrangements of Se and S at the X_a sites and smaller features corresponding to the contributions from the X_b chalcogens to the Li site energy. The magnitude of ε_a controls the position of the three dominant peaks while the magnitude of both ε_b and U control how fast the peaks with a given $n_a\varepsilon_a$ move with z. The widths of the peaks is largely a result of the effective interaction constant p_aU. We tried more complicated forms of the interaction, such as interactions that depend on the value of n_a of the occupied sites, but none of these improved the agreement. The problem is that for $\varepsilon = 1.2kT_g$, n_a is 2 for almost all of the sites when z_a is larger than 6. Therefore, $-(\partial x/\partial V)_T$ should be almost as sharp for $z=6$ and $z=7$ as for $z=8$, unless the magnitude of U decreases by a factor of 3 when z changes from 8 to 7 or 6. We do not know why such a large change should occur.

We can rule out an inhomogeneous sample as the cause of the broadening in $-(\partial x/\partial V)_T$ for $z=7$. Inhomogeneities, such as variations in stoichiometry or in the amount of residual Cu, could lead to a difference between the site energies in different regions of the host. The differences in site energies required to explain our results, however, are unreasonable. If U is the same for $z=7$ as for $z=8$, then a distribution of site energies over a range of about $4kT$ is needed for the theory to match the experiment for $z=7$. Such inhomogeneities in the site energy would imply that at a given voltage, there should be inhomogeneities in the local value of x and so inhomogeneities in the lattice parameters of the host. A spread in site energies of $4kT$ would produce inhomogeneities in x over a range of almost $\Delta x = 1$ when the average x is $\frac{1}{2}$. But from the width of our diffraction peaks and the rate at which the peaks shift with x, we estimate that any inhomogeneities in x must be less than $\Delta x = 0.05$.

Our results show that the chalcogens in $Li_xMo_6Se_zS_{8-z}$ affect the site energy of only nearby Li atoms. If each chalcogen affected many Li atoms, there would be only one site energy, determined by the average number of S and Se in the host. Then $-(\partial x/\partial V)_T$ between $x=0$ and $x=1$ for any z would be a single peak, centered on a voltage intermediate between that of the peaks for the limits $z=0$ and $z=8$. This might happen if the variation in site energy arises from changes in the host bands when S replaces Se. Our results rule out such an "average-crystal" model for the site energy.

C. Lattice expansions

For the two compounds we checked, $Li_xMo_6Se_2S_6$ and $Li_xMo_6Se_6S_2$ (Fig. 4, Table II), the expansion of the host as lithium is intercalated to $x=1$ in $Li_xMo_6Se_zS_{8-z}$ is in

a range covered by the end members $Li_xMo_6Se_8$, which expands by 2.8%,[14] and $Li_xMo_6Se_8$, which expands by 1.7%.[15] We explain the nonlinear variation of the expansion as a function of x by assuming the lattice expansion caused by a Li atom depends on the value of n_a for the site it occupies. Thus, we obtain the curves in Fig. 4, as follows.

We estimate the volume expansions for $n_a=0,1,2$ from the experimental results on $Li_xMo_6Se_8$ (Ref. 14) and $Li_xMo_6S_8$.[15] Let $\Delta v_{n_a=2}$ and $\Delta v_{n_a=0}$ be the volume expansion between $x=0$ to 1 for $Li_xMo_6Se_8$ and $Li_xMo_6S_8$, respectively. An estimate of $\Delta v_{n_a=1}$ is the average, $(\Delta v_{n_a=2}+\Delta v_{n_a=0})/2$. The volume of any intermediate member in $Li_xMo_6Se_zS_{8-z}$ with fixed z is

$$v(x)-v(0)=\sum_{n_a} p_a(n_a)\Delta v_{n_a}\sum_{n_b} p_b(n_b)x_{n_a,n_b} , \tag{13}$$

where $v(0)$ is the volume at $x=0$ and $x_{n_a,n_b}=x_\alpha$ is the fraction of sites $\alpha=(n_a,n_b)$ occupied by Li. These values were calculated from Eqs. (9) and (10) for $p_a(n_a)$ and $p_b(n_b)$ determined from the crystal growing model. Since α_R is near 90°, a similar result holds for the cell edge $a_R(x)$. The lattice expansions predicted for $Li_xMo_6Se_2S_6$ and $Li_xMo_6Se_6S_2$ are the solid curves in Fig. 4(c). The changes in the rhombohedral distances, $\Delta a_R=0.063$ Å ($n_a=2$) and $\Delta a_R=0.040$ Å ($n_a=0$), were taken from the results for $z=8$ (Ref. 14) and $z=0$.[15]

Equation (13) can be used to calculate how the expansion between $x=0$ and $x=1$ depends on z. Unfortunately, an insufficient amount of *in situ* x-ray diffraction data have been collected in the series $Li_xMo_6Se_zS_{8-z}$, but we can use the results obtained by Tarascon *et al.*[13] for the series $TlMo_6Se_zS_{8-z}$. Their Chevrel compounds were prepared by growing $Cu_2Mo_6Se_zS_{8-z}$ at 1200 °C, chemically removing the copper, and inserting thallium at ~500 °C.

The unit-cell volumes for $TlMo_6Se_zS_{8-z}$ and $Mo_6Se_zS_{8-z}$ from Ref. 13 are plotted in Fig. 10(a), and the volume difference $v(1)-v(0)$ is shown as solid circles in Fig. 10(b). This difference is just Eq. (13) with $x=1$, so

$$\begin{aligned} v(1)-v(0)&=\sum_{n_a} p_a\Delta v_{n_a} \\ &=z_a^2\Delta v_{n_a=2}+2z_a(1-z_a)\Delta v_{n_a=1} \\ &\quad +(1-z_a)^2\Delta v_{n_a=0} . \end{aligned} \tag{14}$$

If $\Delta v_{n_a=1}=(\Delta v_{n_a=2}+\Delta v_{n_a=0})/2$, then Eq. (14) becomes

$$v(1)-v(0)=z_a\Delta v_{n_a=2}+(1-z_a)\Delta v_{n_a=0} . \tag{15}$$

The curves in Fig. 10(b) show Eq. (15) for two different crystal growing energies, $\varepsilon=1.2kT_g$ and $\varepsilon=1.65kT_g$. The value of $\varepsilon=1.65kT_g$ gives the best least-squares fit of Eq. (15) to the experiment results from Ref. 13. This agreement between theory and experiment shows that in these compounds, prepared under conditions similar to the ones used in this work, Se prefers sites on the $\bar{3}$ axis.

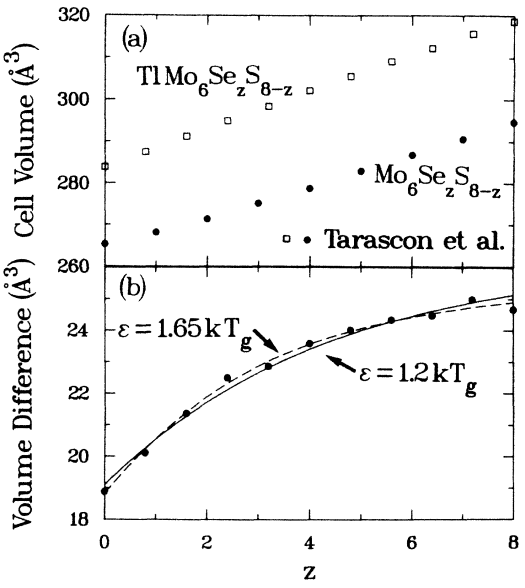

FIG. 10. (a) Rhombedral unit cell volumes for $TlMo_6Se_zS_{8-z}$ (open squares) and $Mo_6Se_zS_{8-z}$ (solid circles) from Ref. 13 plotted as a function of z, the selenium content. (b) Volume difference as a function of z. Solid circles are volume differences calculated from data in (a). The curves are calculated using the lattice-gas model described in the text; solid curve, $\varepsilon=1.2kT_g$; broken curve, $\varepsilon=1.65kT_g$.

D. Triclinic distortions

At room temperature, the structures of both $Li_xMo_6S_8$ and $Li_xMo_6Se_8$ are distorted from rhombohedral to triclinic at $x=4$;[14,15] furthermore, $Li_xMo_6Se_8$ has a second triclinic distortion near $x=2.5$.[14] When these triclinic structures form as x varies, peaks appear in $-(\partial x/\partial V)_T$. We see no evidence for such distortions in the intermediate members of the series $Li_xMo_6Se_zS_{8-z}$, either in $-(\partial x/\partial V)_T$ or with x-ray diffraction.

These triclinic distortions may be associated with an ordered arrangement of the guest atoms on the sites. Such is the case in the triclinic phases of $Cu_{1.8}Mo_6S_8$ (Ref. 24) and $Fe_2Mo_6S_8$.[25] There, each hexagon of inner sites contains two atoms, located diagonally across the hexagon. If we imagine a line joining these two atoms, then there are three orientations for this line in each hexagon. In the triclinic phase, these lines are parallel throughout the crystal. McKinnon and Dahn[26] have proposed two ordered arrangements of Li for the triclinic structures at $x=4$, and have used a lattice-gas model to explain the transition to the ordered state. In both ordered states, the arrangement of atoms in each unit cell is parallel throughout the crystal, in analogy with $Cu_{1.8}Mo_6S_8$ and $Fe_2Mo_6S_8$.

In the models, the ordered state forms to avoid repulsive interactions between the intercalated atoms. The models assume all inner sites have the same energy and so do all outer sites. Aligning the arrangement of atoms in each unit cell thus costs entropy but not energy. In the mixed chalcogenides, however, there is a distribution of

site energies for a given type of site. Thus, in a given unit cell, the different orientations of the ordered arrangement of intercalated atoms no longer have the same energy. If these arrangements of atoms are aligned throughout the crystal, atoms in some unit cells will be forced to occupy unfavorable sites, so the alignment will cost energy as well as entropy. The ordered state will not form if the cost in energy is overly high. We suggest that is this distribution in site energies that suppresses the triclinic states in mixed chalcogenides $Li_xMo_6Se_zS_{8-z}$, $z \neq 0$ or $z \neq 8$.

VI. CONCLUSION

We have studied how a varying chalcogen environment affects intercalated lithium atoms in the series of Chevrel phases, $Li_xMo_6Se_zS_{8-z}$. The lithium site energy is dominated by the two nearest-neighbor chalcogens on the rhombohedral $\bar{3}$ axis. Using electrochemical data, we determined the fraction of sites on the $\bar{3}$ axis occupied by 0, 1, or 2 selenium atoms for a total Se concentration z. We confirmed these results by single-crystal x-ray diffraction, and accounted for them with a model of crystal growth. The occupancy of the chalcogen sites was used in a lattice-gas model to predict the shape of the voltage curves in the electrochemical cells $Li/Li_xMo_6Se_zS_{8-z}$.

ACKNOWLEDGMENT

We would like to thank M. R. Miedema for the chemical analysis.

*Present address: Moli Energy Ltd., 3958 Myrtle Street, Burnaby, British Columbia, Canada V5C 4G2.

[1]S. T. Coleman, W. R. McKinnon, and J. R. Dahn, Phys. Rev. B **29**, 4147 (1984).

[2]R. B. McLellan, Acta Metall. **30**, 317 (1982).

[3]R. Chevrel, M. Sergent, and J. Prigent, J. Solid State Chem. **3**, 515 (1971).

[4]K. Yvon, in *Current Topics in Materials Science,* edited by E. Kaldis (North-Holland, Amsterdam, 1979), Vol. 3, p. 53.

[5]R. Chevrel and M. Sergent, in *Superconductivity in Ternary Compounds I,* Vol. 32 of *Topics in Current Physics,* edited by Ø. Fisher and M. B. Maple (Springer-Verlag, Berlin, 1982), p. 25.

[6]J. R. Dahn and W. R. McKinnon, Solid State Ionics **14**, 131 (1984).

[7]D. W. Murphy, C. Cros, F. J. DiSalvo, and J. V. Waszczak, Inorg. Chem. **16**, 3027 (1977).

[8]J.-M. Tarascon, J. V. Waszczak, G. W. Hull, Jr., F. J. DiSalvo, and L. D. Blitzer, Solid State Commun. **47**, 973 (1983).

[9]D. C. Dahn and R. R. Haering, Solid State Commun. **44**, 29 (1982).

[10]J. R. Dahn and W. R. McKinnon, J. Electrochem. Soc. **131**, 1823 (1984).

[11]W. R. McKinnon and J. R. Dahn, Solid State Commun. **52**, 245 (1984).

[12]J. R. Dahn, M. A. Py, and R. R. Haering, Can. J. Phys. **60**, 307 (1982).

[13]J.-M. Tarascon, F. J. DiSalvo, J. V. Waszczak, and G. W. Hull, Jr., Phys. Rev. B **31**, 1012 (1985); **31**, 8280 (1985).

[14]J. R. Dahn, W. R. McKinnon, and S. T. Coleman, Phys. Rev. B **31**, 484 (1985).

[15]W. R. McKinnon and J. R. Dahn, Phys. Rev. B **31**, 3084 (1985).

[16]W. R. McKinnon and R. R. Haering, in *Modern Aspects of Electrochemistry,* edited by R. E. White, J. O. M. Bockris, and B. E. Conway (Plenum, New York, 1983), Vol. 15, p. 235.

[17]C. Perrin, R. Chevrel, M. Sergent, and Ø. Fisher, Mater. Res. Bull. **14**, 1505 (1979).

[18]D. G. Hinks, J. D. Jorgensen, and H.-C. Li, Phys. Rev. Lett. **51**, 1911 (1983).

[19]F. S. Delk, II and M. J. Sienko, Inorg. Chem. **19**, 788 (1980).

[20]F. S. Delk, II and M. J. Sienko, Inorg. Chem. **19**, 1352 (1980).

[21]J.-M. Tarascon, D. C. Johnson, and M. J. Sienko, Inorg. Chem. **21**, 1505 (1982).

[22]D. C. Johnson, J.-M. Tarascon, and M. J. Sienko, Inorg. Chem. **22**, 3773 (1983).

[23]J. R. Dahn and W. R. McKinnon (unpublished).

[24]K. Yvon, R. Baillif, and R. Flükiger, Acta Cryst. B **35**, 2859 (1980).

[25]K. Yvon, R. Chevrel, and M. Sergent, Acta Cryst. B **36**, 685 (1980).

[26]W. R. McKinnon and J. R. Dahn, J. Phys. C (to be published).